Automatic detection of equiaxed dendrites using computer vision neural networks

A. Viardin*, K. Nöth, M. Torabi Rad, L.Sturz

ACCESS e.V., Intzestrasse 5, D-52072 Aachen, Germany.

arXiv:2207.07428v1 [cond-mat.mtrl-sci] 15 Jul 2022

Abstract

Equaixed dendrites are frequently encountered in solidification. They typically form in large numbers, which makes their detection, localization, and tracking practically impossible for a human eye. In this paper, we show how recent progress in the field of machine learning can be leveraged to tackle this problem and we present computer vision neural network to automatically detect equiaxed dendrites. Our network is trained using phase-field simulation results, and proper data augmentation allows to perform the detection task in solidification conditions entirely different from those simulated for training. For example, here we show how they can successfully detect dendrites of various sizes in a microgravity solidification experiment. We discuss challenges in training such network along with our solutions for them, and compare the performance of neural network with traditional methods of shapes detection.

1. Introduction

Applying methods of artificial intelligence (AI), in particular "deep learning" for software-controlled automated identification, classification and characterization of various characteristics in materials, based on two-dimensional images coming from experimental results has shown a great interest in recent years [1]. In case of *in situ* experimental pictures coming from video sequences, one can have several thousand of pictures to treat in order to extract physical features that are relevant. For this purpose, innovative AI tools must to be developed to overcome the limitations of classical methods of image processing. For solification, several kind of microstructures can be observed during experiments, many of them are dendrites with columnar or equiaxed morphology. The equiaxed dendrites are appearing in isothermal cooling conditions (they are growing in crystallographic directions), while columnar dendrites are growing mainly along a temperature gradient in an elongated form. The objective of this work is the automated detection and characterization of equiaxed dendrites in a melt from time series using deep learning methods. Methods for detection an evaluation for microstructures using machine learning or deep learning techniques are already existing for solidification [2] and solid state transformations [3]. These works shows that neural networks for images detection is already working flawlessly. Deep learning model based on architecture like Faster R-CNN [4], Mask R-CNN [5] or Unet [6] have prooved their ability to detect objects with high accuracy. Nevertheless, the good results concerning objects detection/segmentation/instantiation are depending on the data used to train the network and can be very tedious to generate manually. Especially if one picture contains hundred of objects to detect, annotations of these objects will be very time consuming. The objective of this article is to generate a huge amount of realistic microstructures to train deep learning models. This will be applied to experimental pictures obtained under reduced gravity with resting, focused, growing and later overlapping or connected equiaxed dendrites (experiment "MEDI-2" [7]). Recently Hsu [8], used generative adversarial network to generate 3D microstructures of solid oxide fuel cell electrodes. Here, we have used phase field simulation to generate pictures for training computer vision deep learning architectures in order to analyse experimental microstructures. Phase field models became an important tool for microstructure simulations in the field of solidification with or without fluid flow, solid state transformations or mechanics for example.

*Corresponding author

2. Experimental results

To investigate equiaxed growth of dendrites with <100> crystallographic orientation the binary alloy Neopentylglycol-20.0 wt.% (D)Camphor (NPG-DC) was selected. The phase diagram and relevant alloy properties are given in [9, 10]. The experiment MEDI-2 was carried out on board the sounding rocket TEXUS-55 mission in 2018, where convection of the melt and sedimentation of the dendrites is negligible. The experimental conditions were chosen such as to obtain an equiaxed dendritic structure with diffusive conditions for heat and mass transport during the microgravity period. The dendrites were observed in-situ with two different optical systems to analyze the global and the microscopic features of equiaxed solidification using the TEM 06-23 TEXUS module. As a result, equiaxed dendrites with six dendrite arms growing perpendicular to each other were detected, which is characteristic for a <100> crystallographic orientation. A schematic representation of the TEM 06-23 TEXUS module is shown in Figure 1. This hardware was provided by Airbus Defense & Space. The temperature evolution in the solid or liquid alloy material was measured by three Ni-CrNi thermocouples with diameter 0.25 mm, which were located in the centre vertical plane inside the experimental cell.

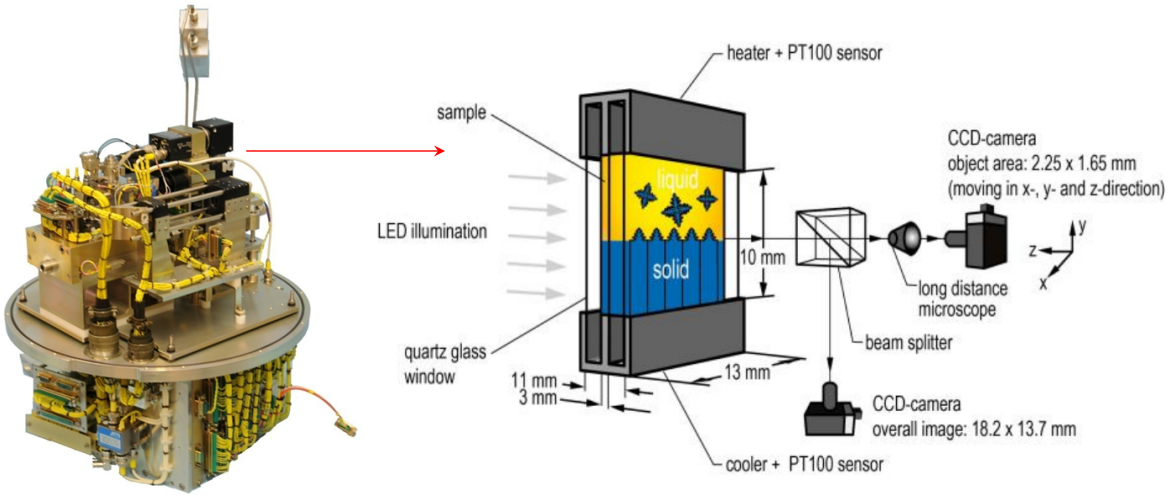


Figure 1: Schematic representation of the TEM 06-23 TEXUS module5.

Figure 2 shows a series of 8-bit greyscale overview images taken with the CCD macro camera. The field of view is 13.6 mm in width and 10.9 mm in height, and the depth-of-field covers the full depth of the sample. The image acquisition rate is 10 frames per second with an optical resolution of 10.625 μm/pixel. Also shown are the thermocouples inserted from the right side.

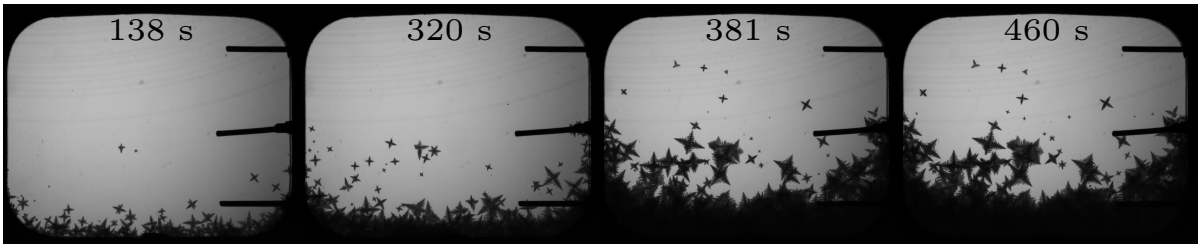


Figure 2: Overview images of the experiment cell showing multiple equiaxed dendritic growth during the microgravity period. Also shown are the thermocouples TZ1 to TZ3 inserted from the right side.

At the beginning of the low-gravity period the NPG-DC alloy is completely liquid. Then, with the experimental parameters chosen, a region with equiaxed dendrites, expands upwards in the experiment cell in a small thermal gradient. The *in-situ* and real-time observation of this process allows for the investigation of the successive nucleation and growth of equiaxed dendrites, remaining at stationary positions in the microgravity environment (Fig. 2).

3. Computer Vision Algorithm

Our objective is to use deep learning neural network to identify and localize each dendrite on each experimental picture as shown in Fig 2. Several architectures already exists for this purpose. Some of the most applied are UNET [6], Mask R-CNN [5] and Faster R-CNN [4]. In this work, we will use Faster R-CNN because of its efficiency and for simple preparation of training data.

3.1. Faster R-CNN

Faster R-CNN is one of the most popular object detection methods. It is part of the R-CNN series, developed by Girshick et al [11], enhanced with Fast R-CNN [12] to finally obtain Faster R-CNN [4]. We only describe the fundamentals of Faster R-CNN here. The input image is passed through a convolutional neural network (CNN) to obtain a feature map of the objects present in the image. This part of Faster R-CNN's architecture is called the "backbone" network. This feature map is then used by a region proposal network (RPN) to generate region proposals (bounding boxes that contain the relevant image objects) using anchors (fixed-size reference boxes placed uniformly in the original image in order to detect the objects). These regions are then filtered by NMS (Non-Maximum Suppression), which is a method that allows to shift through the proposed regions and choose only those that are interesting. The feature map extracted by the CNN and the relevant object bounding boxes are used to generate a new feature map by pooling the regions of interest (RoI). The grouped regions then pass through fully connected layers for object area coordinate prediction and output classes. This part of the Faster R-CNN architecture is called the header network.

3.2. Training and testing

The advantage of this method lies in the generic approach and can be extended to other microstructures if required. Furthermore, a delimitation of the dendrites both by a bounding box and a mask is automatically the outcome of the simulation. In the context of AI and R-CNN, the task is not to simulate the experimental NPG-DC dendrites as physically as possible, but to generate objects that look as similar as possible to the dendrites.

4. Generation of training datasets

4.1. Phase field model

Simulations were performed using the multi-phase field model with obstacle potentials implemented in the software MICRESS [13]. This model [14] is implemented using finite-difference correction method used to improve numerical accuracy [15], and anti-trapping and mobility correction methods [16].

4.2. Simulation parameters

We chose a succinonitrile-1at%acetone alloy for our simulations. Its physical properties are given in Table 1. Growth is initiated from a circular seed at the origin of a 3 dimensional cubic domain. The domain has symmetric boundaries conditions on each face for phase field and alloy concentration. In this way we can simulate only one eight of a dendrite because of its internal symmetry and so reducing calculation time. After the calculation the dendrite is reconstructed by symmetry as we can see on the figure 3. The domain length is 880 μm. The grid is dicretized on finite volume cubic element with a grid spacing of 1μm. The interface thickness is 4 μm. For equiaxed growth, isothermal conditions are used.

The results of one selected simulation are given on Fig. 4 where time evolution of the dendrite morphology is shown. We have performed another simulation with a varying different interface properties. This lead us to a different morphological appearance of the equiaxed dendrite with less pronounced tertiary arms, as we can see on the figures 5 and 6, the dendrite arms are more smooth.

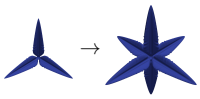


Figure 3: Simulation results at t=1s for 1/8 of a dendrite (isosurface for a phase fraction of 0.5), reconstruction of the whole dendrite by symmetry

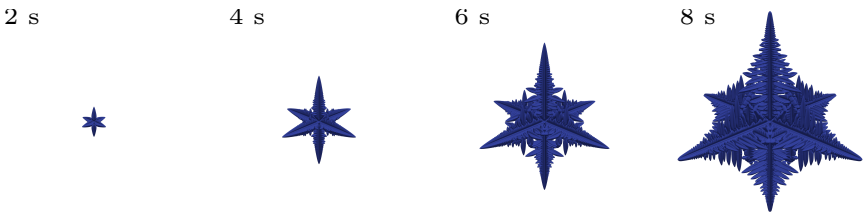


Figure 4: Simulated time evolution of reconstructed dendrite by symmetry

Acetone concentration (C_O)	1at. %
Melting temp. of pure SCN (T_f)	331.231 K
Liquidus slope (m_L)	-2.1 K at.%$^{-1}$
Partition coefficient (k)	0.1
Diffusion coefficient in liquid (D_l)	$1.27{\cdot}10^{-9}$ m^{2}s^{-1}
Diffusion coefficient in solid (D_s)	$3{\cdot}10^{-13}$ m^{2}s^{-1}
Gibbs-Thompson coefficient (Γ)	$6.525 \cdot 10^{-8}$ Km
Interfacial energy (σ_{sl})	$6.525 \cdot 10^{-2}$ Jm^{-2}

Table 1: Thermophysical properties of the SCN-acetone alloy [17]

4.3. Generation of training and test dataset

The results of 3D simulations (isocontour for a phase fraction of 0.5) are presented on the figures 5 and 6 for respectively anisotropy of interfacial energy value of ϵ=0.105 and ϵ=0.01, and isothermal temperature of T = 328 K (undercooling of 1.13 K) and T = 328.67 K (undercooling of 0.46 K). As we can see, the equiaxed dendrite on Fig. 6 have dendritic arms with smaller tip radii and needle like tertiary arms compared to 5. The objective here is to have the two types of dendrites that we see in the experiments with differents kind of arm morphologies.

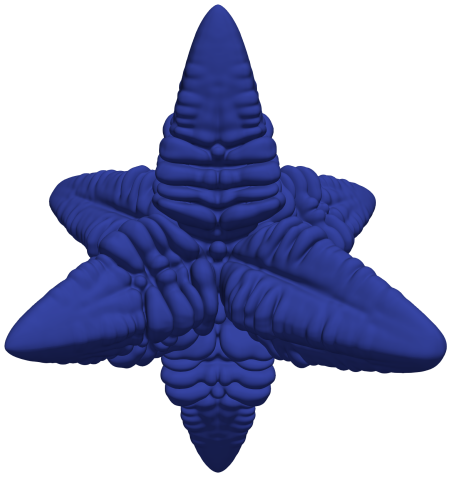


Figure 5: Artificial equiaxed dendrite generated with the phase field method. The interfacial energy anistropy (ϵ_{sl}) is 0.7% and the isothermal temperature is 328 K.

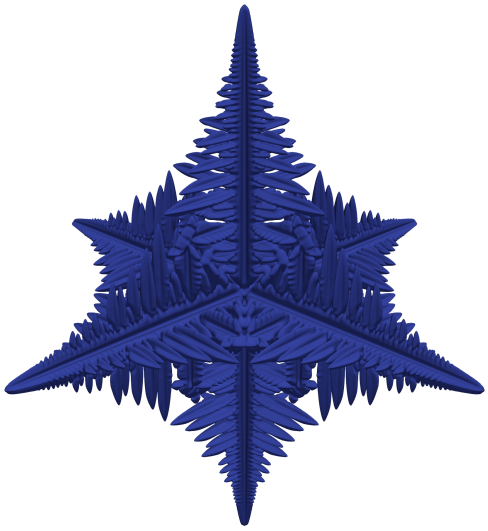


Figure 6: Artificial equiaxed dendrite generated with the phase field method. The interfacial energy anistropy (ϵ_{sl}) is 0.07% and the isothermal temperature is 328.67 K.

From these simulations results various 2D projections can be generated with different camera angle (using paraview scripting) as we can see on the figure 7.

The projections are additionally stretched, overlapped, resized and rotated (augmentation) and

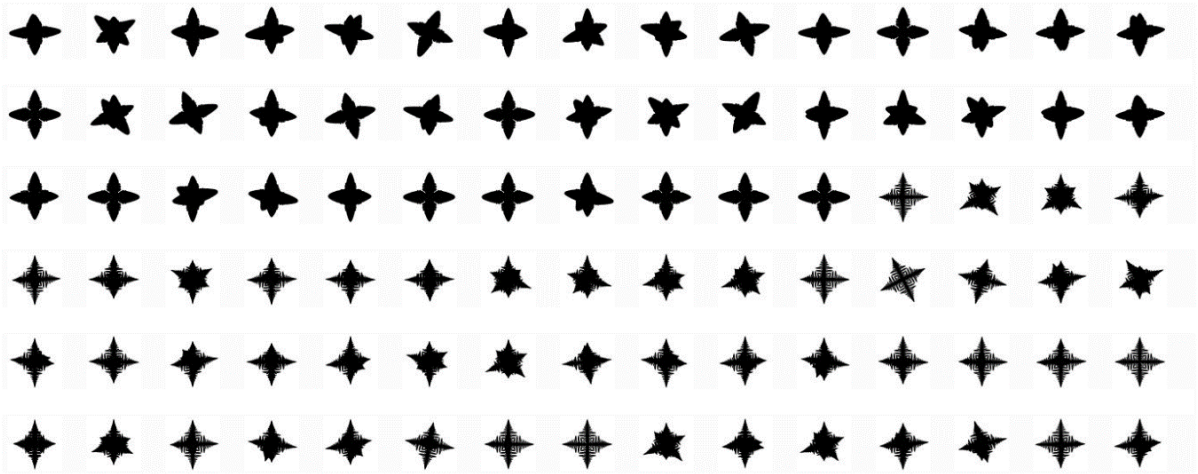


Figure 7: Different projections of the simulated 3D dendrites from Fig. 5.

anchored at random positions. A bounding box is generated and the class indexed ("1") for equiaxed dendrites. In addition, an artificial black bar was generated to depict the thermocouples. The detection of the thermocouples as separate objects has not yet been carried out. A result for a training image is shown in Fig. 8. The Fig. 9 is the same as Fig. 8 but we have plotted the bounding boxes that are saved in the annotations files.

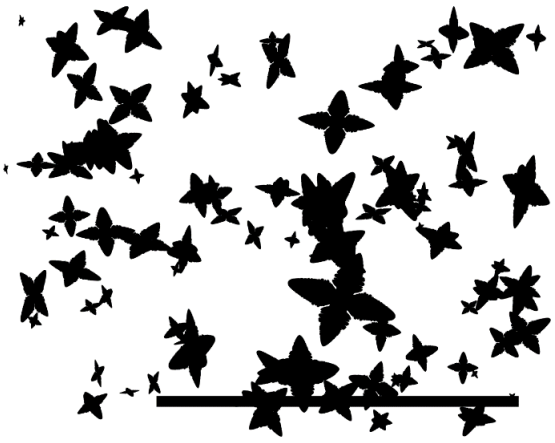


Figure 8: Example of a training image with augmented objects.

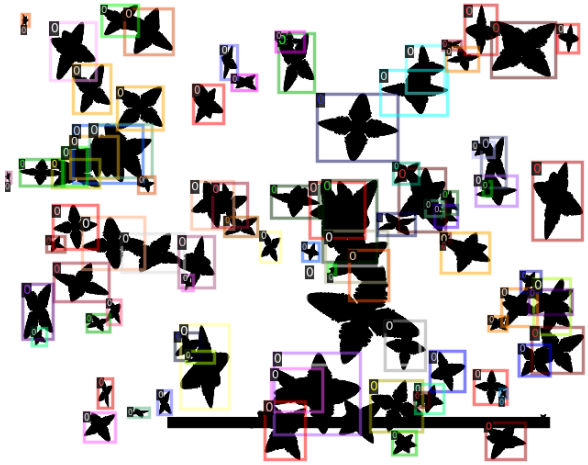


Figure 9: Example of a training image with augmented objects and automatically generated bounding boxes

5. Faster R-CNN

5.1. Model implementation

The Faster R-CNN architecture was implemented using the framework Detectron2, which is an open-source environment for AI. Detectron2 [18] is a library from Facebook© that provides state-of-the-art algorithms for object detection and segmentation and often pre-trained general models. For our project we use a ResNet50 network with FPN (Feature Pyramid Network) as backbone.

5.2. Training and testing parameters

We have generated 80000 pictures, such as Fig. 8 for training coming from phase field results. The dataset for testing were done using 10 pictures, like in Fig. 2 coming from experiments with annotations. The parameter for the Faster R-CNN architecture are listed in the Tab. 2. The training was perfomed on a NVIDIA RTX 6000 GPU and last less than 48 hours.

Image per batch	2
Base learning rate	0.003
Warmup iterations	100
Checkpoint Period	10000
Maximum iterations	130000
Steps	(30000,50000,100000)
Gamma	0.5
Momentum	0.9
ROI heads/Batch size per image	128
Detections per Image	150
Evaluation period	1000

Table 2: Parameter for the Faster R-CNN implemented with Detectron2 [18]

5.3. Results of Faster R-CNN detection

On the figure 10, we have plotted on the left column, the bounding box surrounding dendrites detected using traditional detection method (i.e with matlab) in red. On the right of the Fig. 10 we have plotted the bounding boxes surounding dendrites detected using Faster R-CNN. On each bounding box, the class probability is also given, it is in almost all of the cases close to 100%, this means that the probability that the detected object is a dendrite is around 100% which is true in our case.

In general, the results are very promising. Nevertheless, small remarks have to be done :

- Very small dendrite at the beginning of experiments i.e 220 s are not well detected by Faster R-CNN
- Faster R-CNN detects dendrites near the columnar front and overlapping dendrites much better than classical methods
- There are artefacts with both methods: with the classic method, e.g. at the bottom right and with Faster R-CNN, a false positive object is detected in the upper right image area where the top thermocouple is located
- When dendrites are strongly packed in the bottom of the experimental device, it is hard to detect them for the traditional method as well for Faster R-CNN algorithm

For a more detailed analysis, the evolution with time of the number of dendrites detected was evaluated for the classical method and Faster R-CNN and plotted in the figure 11 as well for the average bounding box area on figure 12. The artifacts were manually removed concerning the classical method as well for Faster R-CNN. For the evolution of the number of dendrites with time, one can see at early stage i.e between 150 and 300 seconds the number of dendrites detected by the classical method is higher than Faster R-CNN because Faster R-CNN did not detect very small dendrites in our first model, while classical methods did. as classical method does. But at larger time i.e superior to 300 s, it is opposite. Faster R-CNN detects more dendrites than the classical method, at this stage Faster R-CNN detects overlapping dendrites better than the classical method and gives a realistic description of the number of dendrite in this experiment. The same observation can be made for the average bounding box area in figure 12, the better detection of packed/overlapping dendrites with Faster R-CNN method drive to higher average bounding box at latter stage of the experiments.

5.4. Conclusion

In this work we have presented a computer vision detection algorithm based on the Faster R-CNN model trained using phase field model results for experimental picture analysis. We have shown that the detection using Faster R-CNN provides better results than a conventional method using shape/edge detection. The Faster R-CNN was implemented using Detectron2 [18]. The advantage is a limited number of phase field simulations or annotations of experimental images. Just with two phase field

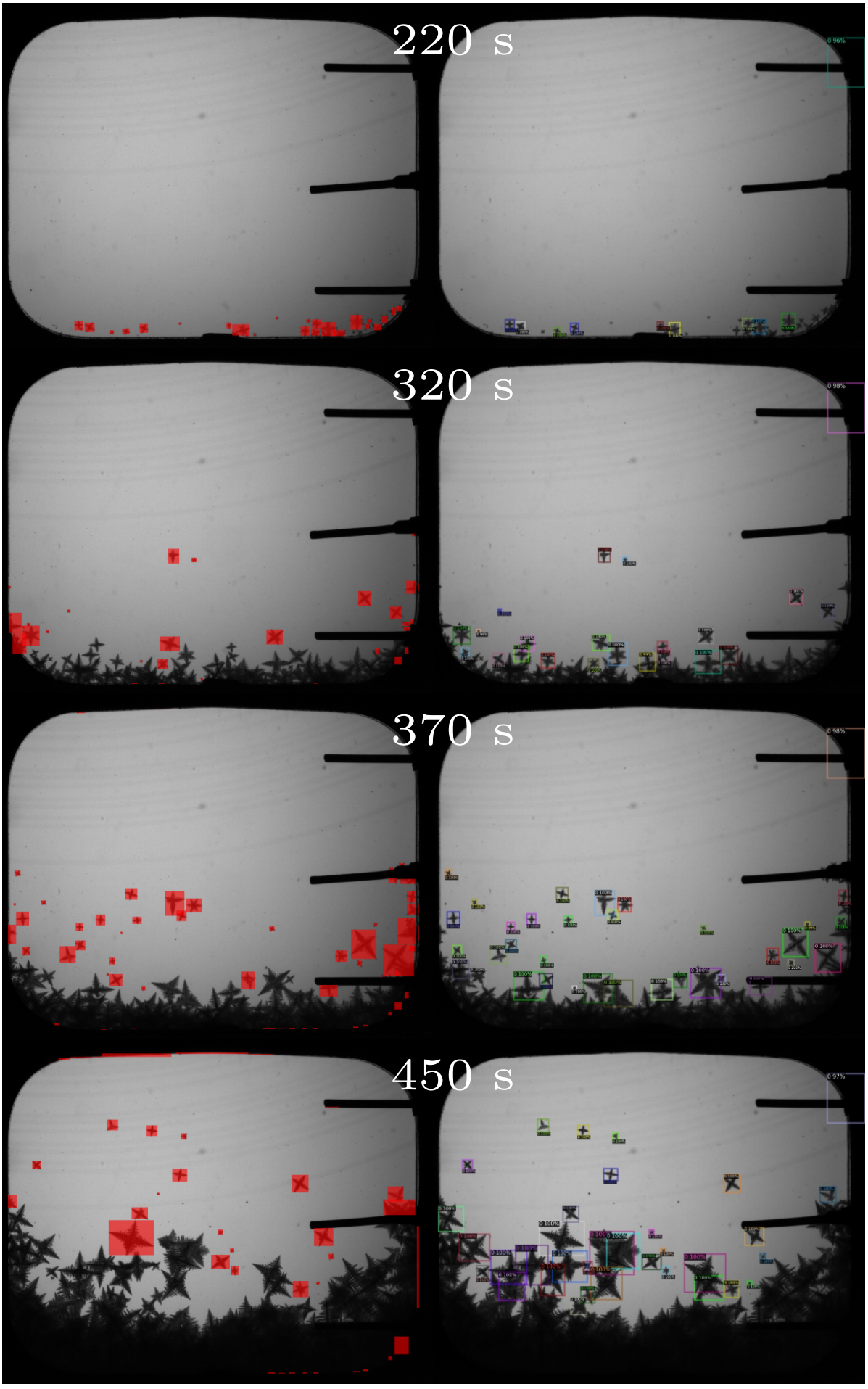


Figure 10: Comparison of classic detection, each on the left, and detection with faster R-CNN, each on the right, with selected image times: 220 s, 320 s, 370s, 450s.

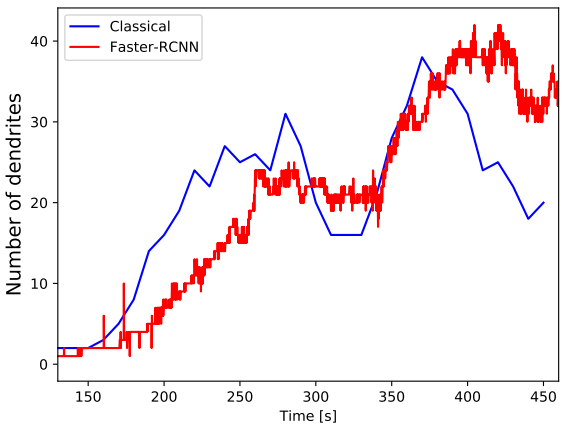


Figure 11: Number of detected dendrites from of the experiment duration

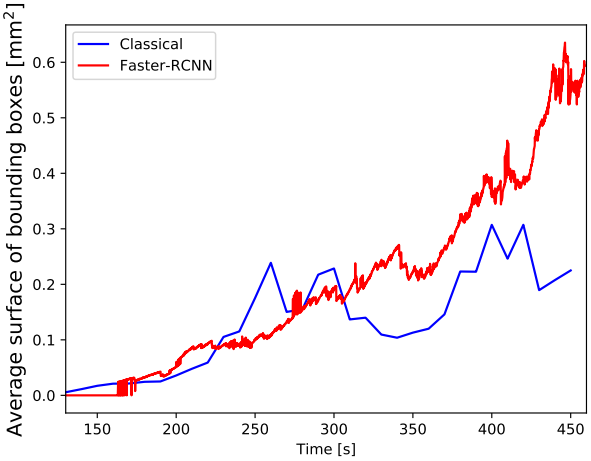


Figure 12: Determined box area of detected dendrites from as a function of the experiment duration

simulations we are able to generate a lot of data for training with realistically looking dendrites. This method can be now applied to classify different solidification morphology like columnar dendrites or seaweed dendrites using training with phase field model results.

5.5. Acknowledgements

This work was financially supported by DLR (Project KICK-G, contract number FKZ50WM2050). The authors want to thank Dr. Markus Apel for fruitful discussion on phase field model.

References

[1] Elizabeth A. Holm, Ryan Cohn, Nan Gao, Andrew R. Kitahara, Thomas P. Matson, Bo Lei, and Srujana Rao Yarasi. Overview: Computer vision and machine learning for microstructural characterization and analysis. *Metallurgical and Materials Transactions A*, 51:5985 – 5999, December 2020.

[2] Enzo Liotti, Carlos Arteta, Andrew Zisserman, Andrew Lui, Victor Lempitsky, and Patrick S. Grant. Crystal nucleation in metallic alloys using x-ray radiography and machine learning. *Science Advances*, 4(4):eaar4004, 2018.

[3] Reuben Agbozo and Wu-Yin Jin. Quantitative metallographic analysis of gcr15 microstructure using mask r-cnn. *Journal of the Korean Society for Precision Engineering*, 37:361–369, 05 2020.

[4] Shaoqing Ren, Kaiming He, Ross B. Girshick, and Jian Sun. Faster R-CNN: towards real-time object detection with region proposal networks. *CoRR*, abs/1506.01497, 2015.

[5] Kaiming He, Georgia Gkioxari, Piotr Dollár, and Ross B. Girshick. Mask R-CNN. *CoRR*, abs/1703.06870, 2017.

[6] Olaf Ronneberger, Philipp Fischer, and Thomas Brox. U-net: Convolutional networks for biomedical image segmentation. *CoRR*, abs/1505.04597, 2015.

[7] Gerhard Zimmermann, Martin Hamacher, and L. Sturz. In-situ observation of equiaxed dendrites solidifying under reduced gravity conditions during the texus-55 mission – the medi-2 experiment. In *Proceedings of the 24rd ESA Symposium on European Rocket and Balloon Programmes and Related Research*, October 2019.

[8] Tim Hsu, William K. Epting, Hokon Kim, Harry W. Abernathy, Gregory A. Hackett, Anthony D. Rollett, Paul A. Salvador, and Elizabeth A. Holm. Microstructure generation via generative adversarial network for heterogeneous, topologically complex 3d materials. *Journal of Materials*, 73, December 2021.

[9] Laszlo Sturz, Mickael Hamacher, Janin Eiken, and Gerhard Zimmermann, editors. *Multiple equiaxed dendrite interaction investigated on MASER-13*, 11-15 June 2017.

[10] Gerhard Zimmermann, Mickael Hamacher, and Laszlo Sturz, editors. *Columnar-to-equiaxed transition in the transparent alloy system NPG-DC observed in the low-gravity and normal gravity experiment TRACE-3*, 11-15 June 2017.

[11] Ross Girshick, Jeff Donahue, Trevor Darrell, and Jitendra Malik. Rich feature hierarchies for accurate object detection and semantic segmentation. In *2014 IEEE Conference on Computer Vision and Pattern Recognition*, pages 580–587, 2014.

[12] Ross B. Girshick. Fast R-CNN. *CoRR*, abs/1504.08083, 2015.

[13] Micress 7. http://www.micress.de.

[14] Janin Eiken, Bernd Böttger, and Ingo Steinbach. Multiphase-field approach for multicomponent alloys with extrapolation scheme for numerical application. *Physical Review E*, 73(6):066122, jun 2006.

[15] Janin Eiken. Numerical solution of the phase-field equation with minimized discretization error. *IOP Conference Series: Materials Science and Engineering*, 33:012105, jul 2012.

[16] Carre A., Böttger B., and Apel M. Implementation of an antitrapping current for a multicomponent multiphase-field ansatz. *J. Cryst. Growth*, 380:5–13, 2013.

[17] Alexandre Viardin, Miha Založnik, youssef Souhar, Markus Apel, and Hervé Combeau. Mesoscopic modeling of spacing and grain selection in columnar dendritic solidification: Envelope versus phase-field model. *Acta Materialia*, 122:386 – 399, January 2017.

[18] Yuxin Wu, Alexander Kirillov, Francisco Massa, Wan-Yen Lo, and Ross Girshick. Detectron2, 2019.